

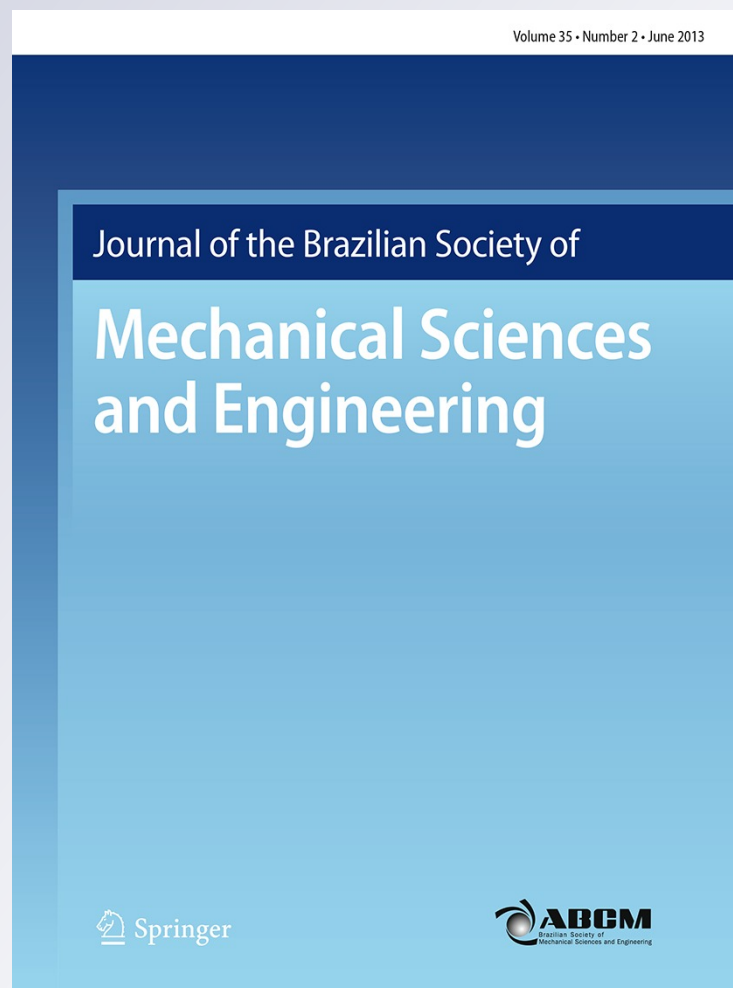
*Implementation of the extended finite element method for coupled dynamic thermoelastic fracture of a functionally graded cracked layer*

**Masoud Mahdizadeh Rokhi & Mahmoud Shariati**

**Journal of the Brazilian Society of Mechanical Sciences and Engineering**

ISSN 1678-5878  
Volume 35  
Number 2

J Braz. Soc. Mech. Sci. Eng. (2013)  
35:69-81  
DOI 10.1007/s40430-013-0015-0



**Your article is protected by copyright and all rights are held exclusively by The Brazilian Society of Mechanical Sciences and Engineering. This e-offprint is for personal use only and shall not be self-archived in electronic repositories. If you wish to self-archive your article, please use the accepted manuscript version for posting on your own website. You may further deposit the accepted manuscript version in any repository, provided it is only made publicly available 12 months after official publication or later and provided acknowledgement is given to the original source of publication and a link is inserted to the published article on Springer's website. The link must be accompanied by the following text: "The final publication is available at [link.springer.com](http://link.springer.com)".**

# Implementation of the extended finite element method for coupled dynamic thermoelastic fracture of a functionally graded cracked layer

Masoud Mahdizadeh Rokhi · Mahmoud Shariati

Received: 18 July 2012 / Accepted: 6 September 2012 / Published online: 3 April 2013  
© The Brazilian Society of Mechanical Sciences and Engineering 2013

**Abstract** The effect of thermal shock on a cracked functionally graded material (FGM) layer is considered using the extended finite element method. Classical coupled thermoelastic equations are used in the calculations. The coupled dynamical system of equations obtained from the extended finite element discretization is solved by the Newmark method in the time domain. Micromechanical models for conventional composites are used to estimate the material properties of functionally graded layer. The interaction integral is then employed to calculate the dynamic thermal stress intensity factors (SIFs) at each time step. The effects of initial crack angle and volume fraction profiles of FGMs on SIFs are studied. Also crack propagation phenomenon is investigated in this paper. We have used MATLAB software to do the different stages of simulation from mesh generation to numerical computation of SIFs. Some numerical examples are implemented to investigate the validity and accuracy of attained results.

**Keywords** Coupled thermoelasticity · Fracture · Thermal shock · Crack propagation · FGMs

## List of symbols

$A$  Element area, area ( $m^2$ )  
 $A^*$  Area associated with the domain  $J$ -integral, area ( $m^2$ )

$a$  Crack length, length (m)  
 $\mathbf{a}$  Vector of nodal unknowns associated with FE shape functions, length (m)  
 $Bf$  Body force vector, force ( $N/m^3$ )  
 $B_x$  and  $B_y$  Body force vector components, force ( $N/m^3$ )  
 $\mathbf{b}$  Vector of nodal unknowns associated with heaviside enriched shape functions, length (m)  
 $\mathbf{c}$  Vector of nodal unknowns associated with crack tip enriched shape functions, length (m)  
 $C$  Damping matrix  
 $C_{ijkl}$  Material constitutive matrix components ( $N/m^2$ )  
 $c_t$  Specific heat capacity [ $J/(kg\ K)$ ]  
 $D$  Material modulus matrix ( $N/m^2$ )  
 $E$  Young's modulus ( $N/m^2$ )  
 $F_m$  Crack tip enrichment functions ( $m^{0.5}$ )  
 $Fr$  Force vector (N)  
 $H$  Heaviside enrichment function, dimensionless  
 $J$   $J$  integral (N/m)  
 $K$  Stiffness matrix  
 $K^{eq}$  Equivalent dynamic stress intensity factor ( $N/m^{1.5}$ )  
 $K_I$  Mode I stress intensity factor ( $N/m^{1.5}$ )  
 $K_{IC}$  Fracture toughness ( $N/m^{1.5}$ )  
 $K_{ID}$  Fracture toughness ( $N/m^{1.5}$ )  
 $K_{II}$  Mode II stress intensity factor ( $N\ m^{1.5}$ )  
 $k$  Thermal conductivity [ $W/(m\ K)$ ]  
 $L$  Length of specimen, length (m)  
 $M$  Mass matrix (kg)  
 $MI$   $M$ -integral (N/m)  
 $m$  Number of crack tip enrichment functions (m)  
 $N$  FEM shape function, dimensionless  
 $n_x$  and  $n_y$  Unit vectors in  $x$  and  $y$  directions  
 $p$  Power exponent determining the volume fraction profiles, dimensionless

Technical Editor: Lavinia Borges.

M. M. Rokhi (✉) · M. Shariati  
Mechanical Engineering Department, Shahrood University  
of Technology, 361995161 Shahrood, Semnan, Iran  
e-mail: masoud\_mahdizadeh@yahoo.com

M. Shariati  
e-mail: mshariati44@gmail.com

$q$	Smoothing weight function, dimensionless
$q_i$	Component of heat flux vector per unit area ( $\text{W}/\text{m}^2$ )
$R$	Generated heat per unit volume ( $\text{W}/\text{m}^3$ )
$r$	Polar coordinate system component, length (m)
$S$	Vector of XFE shape functions
$T$	Temperature (K)
$Tf$	Traction force vector ( $\text{N}/\text{m}^2$ )
$t$	Time (s)
$t_D$	Dimensionless time, dimensionless
$t_x^n$	Traction vector components at x direction ( $\text{N}/\text{m}^2$ )
$t_y^n$	Traction vector components at y direction ( $\text{N}/\text{m}^2$ )
$u$	Displacement vector (m)
$V$	Volume ( $\text{m}^3$ )
$V_i$	Volume fraction of inclusion, dimensionless
$W$	Height of specimen, length (m)
$X$	Global Cartesian coordinate system component
$x$	Local Cartesian coordinate system component

**Greek symbols**

$\alpha$	Coefficient of thermal expansion (1/K)
$\beta$	Coupling term [ $\text{N}/(\text{m}^2 \text{K})$ ]
$\beta_i$	Universal functions, dimensionless
$\gamma$	Coefficient of Newmark method, dimensionless
$\zeta$	Coefficient of Newmark method, dimensionless
$\delta_{ij}$	Kronecker delta, dimensionless
$\varepsilon$	Strain tensor, dimensionless
$\varepsilon^{\text{aux}}$	Auxiliary strain tensor, dimensionless
$\varepsilon_{ij}^m$	Mechanical strain component, dimensionless
$\theta$	Temperature change (K)
$\mu$	Lamé constant ( $\text{N}/\text{m}^2$ )
$\lambda$	Lamé constant ( $\text{N}/\text{m}^2$ )
$\nu$	Poisson's ratio, dimensionless
$\rho$	Density ( $\text{kg}/\text{m}^3$ )
$\varphi$	Polar coordinate system component, dimensionless
$\sigma$	Stress tensor ( $\text{N}/\text{m}^2$ )
$\sigma^{\text{aux}}$	Auxiliary stress tensor ( $\text{N}/\text{m}^2$ )
$\Phi$	Enrichment shape function, dimensionless
$\Psi$	Enrichment shape function, dimensionless
$\omega$	The angle between local and global coordinate systems, dimensionless
$\omega_c$	Crack propagation direction, dimensionless
$\Delta$	Nodal displacements and temperature changes vector

**Subscripts**

$h$	Relative to nodes in an element
$i$	Relative to components of Cartesian coordinate system

$j$	Relative to components of Cartesian coordinate system
$l$	Relative to the shape functions
$m$	Relative to crack tip enrichment functions
$n$	Relative to nodes, time step and component of coordinate system
$ne$	Relative to nodes in element $e$
$ns$	Relative to XFE shape functions
tip	Relative to crack tip
1	Relative to the horizontal axis of coordinate system
2	Relative to the vertical axis of coordinate system

**Superscript**

aux	Relative to auxiliary field
-----	-----------------------------

**1 Introduction**

Functionally graded materials (FGMs) are a new class of composite materials characterized by the gradual variation in microstructure and material properties. FGMs were initially designed as thermal barrier materials for aerospace structural applications and fusion reactors. They are now developed for general use as structural components in extremely high-temperature environments. The ability to predict the response of FGM plates and shells when subjected to thermal and mechanical loads is of prime interest to structural analysis. FGM components are generally constructed to sustain severe temperature gradients. Continuously varying the volume fraction of the mixture in the FG materials eliminates the interface problems and alleviates thermal stress concentrations and causes a more smooth stress distribution [1]. Ceramic materials, because of their excellent properties at high temperatures and their superior wear and corrosion resistance, are used widely in structure of FGMs. One major limitation of ceramics is their intrinsic brittleness that can result in fracture under severe thermal shocks. Therefore, the fracture analyses of FGMs under thermal shocks are important to their permanence in engineering applications.

To adapt the standard finite element method to fracture computations, the extended finite element method (XFEM) has been developed which completely avoids remeshing [3, 4, 26]. Also see Stolarska et al. [32] where it was combined with level sets. This XFEM is based on the partition of unity [24]. In this method, a discontinuous enrichment function is used along the crack path to describe a discontinuous displacement [26].

The response of functionally graded cracked layers under thermal shocks is found in just a few articles. Noda [28] and Fujimoto and Noda [8, 9] have done a series of works on using the finite element method to obtain the crack stress intensity factors (SIFs) under thermal loading

conditions. They considered homogeneous and FGMs and examined the influence of material gradation and thermal shock on crack propagation. They considered the heat conduction equation where thermo-coupling has been ignored. Lee and Erdogan [23], Bao and Cai [2], Lee and Erdogan [22], Quian et al. [29] and Gaudette et al. [10] focused on investigation of delamination and cracking of FGMs at coating-substrate interfaces due to thermal loads. Jin and Paulino [18] studied an edge crack in a strip of a FGM under transient thermal loading conditions. They employed a multi-layered material model to obtain the temperature field. Hosseini-Tehrani et al. [14] and Hosseini-Tehrani et al. [15] employed the boundary element method to investigate the effect of the coupling and inertia terms in dynamical thermal loading problems.

Duflot [5] investigated the static case of thermoelastic fracture by XFEM where both 2D and 3D problems with different crack face thermal boundary conditions are included. Kc and Kim [19], using the finite element method evaluated the non-singular T-stress and mixed-mode SIFs in FGMs under steady-state thermal loads via interaction integral. Zamani and Eslami [35] employed the finite element method to obtain the SIF for a functionally graded cracked body under coupled classical thermoelastic assumption. They assumed that the crack remains stationary within simulation. Also the XFEM formulation was implemented by Zamani and Eslami [36] to model the effect of the mechanical and thermal shocks on a cracked body. The crack was assumed to be stationary. Feng and Jin [7] examined the fracture behavior of an FGM plate containing parallel surface cracks with alternating lengths subjected to a thermal shock. Ekhlakov et al. [6] developed a boundary-domain element method (BDEM) for a transient thermoelastic crack analysis in isotropic, continuously non-homogeneous and linear elastic FGMs. They considered a stationary edge crack in a two-dimensional finite domain subjected to a thermal shock and computed SIFs.

The study of crack propagation phenomena in a functionally graded cracked layer under thermal shock and using the coupled thermoelastic equations is not found in previous articles. In present study, the XFEM formulation is implemented to model the effect of thermal shocks on a functionally graded cracked layer under coupled classical thermoelastic assumption. The Newmark time integration scheme is used to solve the dynamical system of matrix equations obtained from the spatial discretization of initial coupled equations. The most general form of interaction integral for FGMs is extracted based on the non-equilibrium formulation and also dynamical SIFs are computed in each time step. A MATLAB code is developed to implement the different stages of computation from mesh generation to calculation of the SIFs and crack propagation simulation. Some numerical examples are implemented to

investigate the validity and accuracy of the written computer program. The effects of initial crack angle and volume fraction profiles of FGMs on the SIFs are investigated in this paper. The crack is assumed to be moving under a thermal shock higher than its critical value. Also crack propagation phenomenon is considered which seems not to be reported with this condition in previous works.

## 2 General problem formulation

### 2.1 Space discretization

The general governing equations of the classical coupled thermoelasticity are the equation of motion (Eq. 1) and the first law of thermodynamics (Eq. 2), as [13].

$$\sigma_{ij,j} + B_i = \rho \ddot{u}_i \tag{1}$$

$$q_{i,i} + \rho c_i \dot{\theta} + T_0(1 + \theta/T_0)\beta \dot{\epsilon}_{ii} = R \tag{2}$$

If the temperature change ( $\theta$ ) is small compared to the reference temperature  $T_0$ , Eq. (2) may be approximately written in the simpler form [13].

$$q_{i,i} + \rho c_i \dot{\theta} + T_0 \beta \dot{\epsilon}_{ii} = R \tag{3}$$

The system of coupled equations 1 and 2 does not have a general analytical solution. The extended finite element model of the problem is obtained by discretizing the solution domain into a number of arbitrary elements. In the XFEM formulation, a standard local displacement approximation around the crack is enriched with discontinuous jump function across the crack faces and the asymptotic crack tip displacement field around the crack tip [4]. The same procedure is used for the temperature enrichment [5]. The formulation of the XFEM for displacement components can be written as [36]

$$\begin{aligned} \mathbf{u}(x, y, t) = & \sum_N N_n(x, y) \mathbf{a}_n(t) + \sum_{n \in N_{cr}} N_n(x, y) [H(x, y) \\ & - H(x_n, y_n)] \mathbf{b}_n(t) + \sum_m \sum_{n \in N_{tip}} N_n(x, y) [F_m(r, \varphi) \\ & - F_m(r_n, \varphi_n)] \mathbf{c}_{nm}(t) \end{aligned} \tag{4}$$

where  $N_{cr}$  is the set of nodes that the discontinuity has in its influence domain, while  $N_{tip}$  is the set of nodes inside a predefined area around the crack tip (see Fig. 1). Here,  $H(x, y)$  is Heaviside enrichment function and  $\{F_m\}$  represents crack tip enrichment functions.

$$\{F_m\} = \{r^{0.5} \sin(\varphi/2), r^{0.5} \cos(\varphi/2), r^{0.5} \sin(\varphi) \sin(\varphi/2), r^{0.5} \sin(\varphi) \cos(\varphi/2)\} \tag{5}$$

where  $r$  and  $\varphi$  are the usual crack tip polar coordinates. Also  $\mathbf{a}_n(t) = \{a_n^u(t), a_n^v(t)\}^T$ ,  $\mathbf{b}_n(t) = \{b_n^u(t), b_n^v(t)\}^T$  and  $\mathbf{c}_{nm}(t) = \{c_{nm}^u(t), c_{nm}^v(t)\}^T$  are vectors of nodal unknowns.

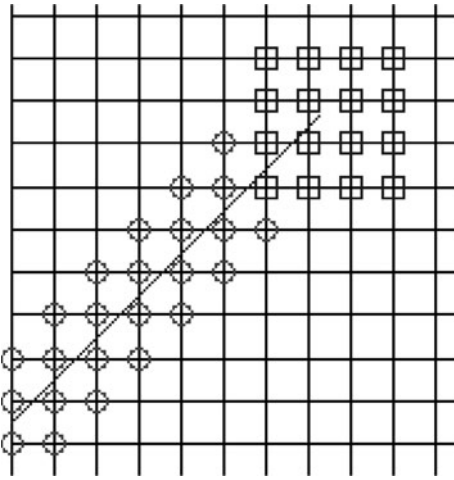


**Fig. 1** Selection of enriched nodes for edge crack. *Circled nodes* are enriched by the discontinuity function whereas the *squared nodes* are enriched by the crack tip enrichment functions

In this study, the crack faces are assumed to be adiabatic so the temperature is discontinuous along the crack faces and the heat flux is singular at the crack tip. Thus, the temperature field is discretized similar to the displacement field, but only with the first crack tip enrichment function [36].

$$\theta(x, y, t) = \sum_{\text{all nodes}} N_n(x, y) a_n^T(t) + \sum_{n \in N_{cr}} N_n(x, y) [H(x, y) - H(x_n, y_n)] b_n^T(t) + \sum_{n \in N_{tip}} N_n(x, y) [r^{0.5} \sin(\varphi/2) - r^{0.5} \sin(\varphi_n/2)] c_n^T(t) \quad (6)$$

where  $a_n^T(t)$ ,  $b_n^T(t)$  and  $c_n^T(t)$  are the nodal unknowns corresponding to temperature field.

Now, the base element ( $e$ ) with  $n$  nodal points is considered and the displacement components and temperature change in the element ( $e$ ) are approximated by compact forms as follows:

$$\mathbf{u}^e(x, y, t) = N_h(x, y) \mathbf{a}_h^u(t) + \Phi_h(x, y) \mathbf{b}_h^u(t) + \Psi_{hm}(x, y) \mathbf{c}_{hm}^u(t) \quad (7)$$

$$\mathbf{v}^e(x, y, t) = N_h(x, y) \mathbf{a}_h^v(t) + \Phi_h(x, y) \mathbf{b}_h^v(t) + \Psi_{hm}(x, y) \mathbf{c}_{hm}^v(t) \quad (8)$$

$$\theta^e(x, y, t) = N_h(x, y) a_h^T(t) + \Phi_h(x, y) b_h^T(t) + \Psi_{hm}(x, y) c_{hm}^T(t) \quad (9)$$

$h = 1, 2, \dots, ne \quad m = 1, 2, 3, 4$

where  $ne$  is number of nodes in element ( $e$ ) and  $c_{nm}^T(t)$  is component of vector  $\mathbf{c}^T(t)$  defined by

$$\mathbf{c}^T(t) = \{c_{11}^T, 0, 0, 0, c_{21}^T, 0, 0, 0, c_{31}^T, 0, 0, 0, c_{41}^T, 0, 0, 0\} \quad (10)$$

Also  $\Phi$  and  $\Psi$  exhibit the enriched parts of both displacement and temperature fields. They can be related to face and tip enrichment, respectively (Eqs. 11 and 12).

$$\Phi_h(x, y) = N_h(x, y) [H(x, y) - H(x_h, y_h)] \quad (11)$$

$$\Psi_h(x, y) = N_h(x, y) [r^{0.5} \sin(\varphi/2) - r_h^{0.5} \sin(\varphi_h/2), r^{0.5} \cos(\varphi/2) - r_h^{0.5} \cos(\varphi_h/2), r^{0.5} \sin(\varphi) \sin(\varphi/2) - r_h^{0.5} \sin(\varphi_h) \sin(\varphi_h/2), r^{0.5} \sin(\varphi) \cos(\varphi/2) - r_h^{0.5} \sin(\varphi_h) \cos(\varphi_h/2)] \quad (12)$$

Using Eqs. (7)–(9) one can evaluate the first and second derivatives in time (Eqs. (13)–(17)).

$$\dot{\mathbf{u}}^e(x, y, t) = N_h(x, y) \dot{\mathbf{a}}_h^u(t) + \Phi_h(x, y) \dot{\mathbf{b}}_h^u(t) + \Psi_{hm}(x, y) \dot{\mathbf{c}}_{hm}^u(t) \quad (13)$$

$$\ddot{\mathbf{u}}^e(x, y, t) = N_h(x, y) \ddot{\mathbf{a}}_h^u(t) + \Phi_h(x, y) \ddot{\mathbf{b}}_h^u(t) + \Psi_{hm}(x, y) \ddot{\mathbf{c}}_{hm}^u(t) \quad (14)$$

$$\dot{\mathbf{v}}^e(x, y, t) = N_h(x, y) \dot{\mathbf{a}}_h^v(t) + \Phi_h(x, y) \dot{\mathbf{b}}_h^v(t) + \Psi_{hm}(x, y) \dot{\mathbf{c}}_{hm}^v(t) \quad (15)$$

$$\ddot{\mathbf{v}}^e(x, y, t) = N_h(x, y) \ddot{\mathbf{a}}_h^v(t) + \Phi_h(x, y) \ddot{\mathbf{b}}_h^v(t) + \Psi_{hm}(x, y) \ddot{\mathbf{c}}_{hm}^v(t) \quad (16)$$

$$\dot{\theta}^e(x, y, t) = N_h(x, y) \dot{a}_h^T(t) + \Phi_h(x, y) \dot{b}_h^T(t) + \Psi_{hm}(x, y) \dot{c}_{hm}^T(t) \quad (17)$$

$h = 1, 2, \dots, ne \quad m = 1, 2, 3, 4$

Applying the weighted residual integral to the equation of motion (Eq. 1) and the energy equation (Eq. 3) with respect to the weighting functions  $S_l(x, y)$ , the formal Galerkin approximations reduce to

$$\int_{V(e)} (\sigma_{ij,j} + B_i - \rho \ddot{u}_i) S_l dV = 0, \quad l = 1, 2, \dots, ns \quad (18)$$

$$\int_{V(e)} (q_{i,i} + \rho c_i \dot{\theta} + T_0 \beta \dot{u}_{i,i} - R) S_l dV = 0, \quad l = 1, 2, \dots, ns \quad (19)$$

where  $ns$  is the number of shape functions of element ( $e$ ) and  $S_l$  is component of vector

$$\mathbf{S} = \{N_1, N_2, N_3, N_4, \Phi_1, \Phi_2, \Phi_3, \Phi_4, \Psi_{1m}, \Psi_{2m}, \Psi_{3m}, \Psi_{4m}\} \quad (20)$$

$m = 1, 2, 3, 4$

Hooke's law correlates the stress tensor to the displacement components and temperature change  $\theta$  via Eq. (21).

$$\sigma_{ij} = \mu(u_{i,j} + u_{j,i}) + [\lambda u_{k,k} - \beta \theta] \delta_{ij} \quad (21)$$

where  $\beta = \alpha(3\lambda + 2\mu)$  and  $\theta = (T - T_0)$ . According to Fourier's law of heat conduction we have,

$$q_i = -k_{ij} \theta_{,j} \quad (22)$$

where  $k_{ij}$  is the coefficient of thermal conduction for a general anisotropic material. By substituting Eqs. (7)–(9),

(21) and (22) into Eqs. (18) and (19) and using the Gauss divergence theorem, after some manipulations, the following equations for two-dimensional coupled thermoelasticity will be obtained.

$$\begin{aligned}
 & \left( \int_{V(e)} \rho S_l N_h \, dV \right) \ddot{a}_h^u + \left( \int_{V(e)} \rho S_l \Phi_h \, dV \right) \ddot{b}_h^u \\
 & + \left( \int_{V(e)} \rho S_l \Psi_{hm} \, dV \right) \ddot{c}_{hm}^u \\
 & + \left( \int_{V(e)} [(\lambda + 2\mu) S_{l,x} N_{h,x} + \mu S_{l,y} N_{h,y}] \, dV \right) a_h^u \\
 & + \left( \int_{V(e)} [(\lambda + 2\mu) S_{l,x} \Phi_{h,x} + \mu S_{l,y} \Phi_{h,y}] \, dV \right) b_h^u \\
 & + \left( \int_{V(e)} [(\lambda + 2\mu) S_{l,x} \Psi_{hm,x} + \mu S_{l,y} \Psi_{hm,y}] \, dV \right) c_{hm}^u \\
 & + \left( \int_{V(e)} [\lambda S_{l,x} N_{h,y} + \mu S_{l,y} N_{h,x}] \, dV \right) a_h^v \\
 & + \left( \int_{V(e)} [\lambda S_{l,x} \Phi_{h,y} + \mu S_{l,y} \Phi_{h,x}] \, dV \right) b_h^v \\
 & + \left( \int_{V(e)} [\lambda S_{l,x} \Psi_{hm,y} + \mu S_{l,y} \Psi_{hm,x}] \, dV \right) c_{hm}^v \\
 & - \int_{V(e)} \beta S_{l,x} (N_h a_h^T + \Phi_h b_h^T + \Psi_{hm} c_{hm}^T) \, dV \\
 & = \int_{V(e)} B_x S_l \, dV + \int_{A(e)} t_x^n S_l \, dA \\
 \end{aligned} \tag{23}$$

$$\begin{aligned}
 & \left( \int_{V(e)} \rho S_l N_h \, dV \right) \ddot{a}_h^v + \left( \int_{V(e)} \rho S_l \Phi_h \, dV \right) \ddot{b}_h^v \\
 & + \left( \int_{V(e)} \rho S_l \Psi_{hm} \, dV \right) \ddot{c}_{hm}^v \\
 & + \left( \int_{V(e)} [\mu S_{l,x} N_{h,y} + \lambda S_{l,y} N_{h,x}] \, dV \right) a_h^u \\
 \end{aligned}$$

$$\begin{aligned}
 & + \left( \int_{V(e)} [\mu S_{l,x} \Phi_{h,y} + \lambda S_{l,y} \Phi_{h,x}] \, dV \right) b_h^u \\
 & + \left( \int_{V(e)} [\mu S_{l,x} \Psi_{hm,y} + \lambda S_{l,y} \Psi_{hm,x}] \, dV \right) c_{hm}^u \\
 & + \left( \int_{V(e)} [\mu S_{l,x} N_{h,x} + (\lambda + 2\mu) S_{l,y} N_{h,y}] \, dV \right) a_h^v \\
 & + \left( \int_{V(e)} [\mu S_{l,x} \Phi_{h,x} + (\lambda + 2\mu) S_{l,y} \Phi_{h,y}] \, dV \right) b_h^v \\
 & + \left( \int_{V(e)} [\mu S_{l,x} \Psi_{hm,x} + (\lambda + 2\mu) S_{l,y} \Psi_{hm,y}] \, dV \right) c_{hm}^v \\
 & - \int_{V(e)} \beta S_{l,y} (N_h a_h^T + \Phi_h b_h^T + \Psi_{hm} c_{hm}^T) \, dV \\
 & = \int_{V(e)} B_y S_l \, dV + \int_{A(e)} t_y^n S_l \, dA \\
 \end{aligned} \tag{24}$$

$$\begin{aligned}
 & \left( \int_{V(e)} \rho c_l S_l N_h \, dV \right) \ddot{a}_h^T + \left( \int_{V(e)} \rho c_l S_l \Phi_h \, dV \right) \ddot{b}_h^T \\
 & + \left( \int_{V(e)} \rho c_l S_l \Psi_{hm} \, dV \right) \ddot{c}_{hm}^T \\
 & + \left( \int_{V(e)} [k_x S_{l,x} N_{h,x} + k_y S_{l,y} N_{h,y}] \, dV \right) a_h^T \\
 & + \left( \int_{V(e)} [k_x S_{l,x} \Phi_{h,x} + k_y S_{l,y} \Phi_{h,y}] \, dV \right) b_h^T \\
 & + \left( \int_{V(e)} [k_x S_{l,x} \Psi_{hm,x} + k_y S_{l,y} \Psi_{hm,y}] \, dV \right) c_{hm}^T \\
 & + \left( \int_{V(e)} T_0 \beta S_l N_{h,x} \, dV \right) \dot{a}_h^u + \left( \int_{V(e)} T_0 \beta S_l \Phi_{h,x} \, dV \right) \dot{b}_h^u \\
 & + \left( \int_{V(e)} T_0 \beta S_l \Psi_{hm,x} \, dV \right) \dot{c}_{hm}^u + \left( \int_{V(e)} T_0 \beta S_l N_{h,y} \, dV \right) \dot{a}_h^v \\
 \end{aligned}$$

$$\begin{aligned} \dot{quad} + \left( \int_{V(e)} T_0 \beta S_l \Phi_{h,y} dV \right) \dot{b}_h^v + \left( \int_{V(e)} T_0 \beta S_l \Psi_{hm,y} dV \right) \dot{c}_{hm}^v & \{\Delta\}^{(e)} = \{a_h^u, a_h^v, b_h^u, b_h^v, c_{hm}^u, c_{hm}^v, a_h^T, b_h^T, c_{hm}^T\}^T, \\ & h, m = 1, \dots, 4 \end{aligned} \tag{31}$$

$$\begin{aligned} &= \int_{V(e)} RS_l dV - \int_{A(e)} (q_x n_x) S_l dA - \int_{A(e)} (q_y n_y) S_l dA \\ & l = 1, 2, \dots, ns \quad h = 1, 2, \dots, ne \quad m = 1, 2, 3, 4 \end{aligned} \tag{25}$$

where  $ne = 4$  for a four node element. Equations (23)–(25) are assembled into a matrix form resulting in the general finite element coupled equation given by Eq. (26).

$$[M]\{\ddot{\Delta}\} + [C]\{\dot{\Delta}\} + [K]\{\Delta\} = \{Fr\} \tag{26}$$

where  $[M]$ ,  $[C]$  and  $[K]$  are mass, damping, and stiffness matrices, respectively. Generally, for base element ( $e$ ) which is enriched with both Heaviside and crack tip enrichment functions, these matrices can be written as follows:

$$[M]^{(e)} = \begin{bmatrix} [M_1] & [0]_{48 \times 24} \\ [0]_{24 \times 48} & [0]_{24 \times 24} \end{bmatrix} \tag{27}$$

$$[C]^{(e)} = \begin{bmatrix} [0]_{48 \times 48} & [0]_{48 \times 24} \\ [C_1] & [C_2] \end{bmatrix} \tag{28}$$

$$[K]^{(e)} = \begin{bmatrix} [K_1] & [K_2] \\ [0]_{24 \times 48} & [K_3] \end{bmatrix} \tag{29}$$

$\{Fr\}$  is the force vector defined by Eq. (30).

$$\{Fr\}^{(e)} = \left\{ \begin{aligned} &\int_{V(e)} [S]^T \{Bf\} dV + \int_{A(e)} [S]^T \{Tf\} dA \\ &\int_{V(e)} R [St]^T dV - \int_{A(e)} (q_x n_x + q_y n_y) [St]^T dA \end{aligned} \right\} \tag{30}$$

And  $\{\Delta\}$  is the nodal displacements and temperature changes vector (Eq. (31)).

Also  $\{\dot{\Delta}\}$  and  $\{\ddot{\Delta}\}$  are the first and second time derivative of  $\{\Delta\}$ , respectively. Components of mass, damping, and stiffness matrices are obtained as follows:

$$[M_1] = \int_{V(e)} \rho [S]^T [S] dV \tag{32}$$

$$[C_1] = \int_{V(e)} T_0 \beta [St]^T [S_1] dV, \tag{33}$$

$$[C_2] = \int_{V(e)} \rho c_t [St]^T [St] dV \tag{34}$$

$$[K_1] = \int_{V(e)} [S_2]^T [D] [S_2] dV \tag{35}$$

$$[K_2] = - \int_{V(e)} \beta [S_1]^T [St] dV \tag{36}$$

For isotropic materials  $k_x = k_y = k$ , therefore  $[K_3]$  is obtained as follows:

$$[K_3] = \int_{V(e)} k [S_3]^T [S_3] dV \tag{37}$$

Matrices  $[St]$ ,  $[S]$ ,  $[S_1]$ ,  $[S_2]$ ,  $[S_3]$  and vectors  $\{Bf\}$  and  $\{Tf\}$  are derived as follows:

$$[St] = [N_1 \quad \dots \quad N_4 \quad \Phi_1 \quad \dots \quad \Phi_4 \quad \Psi_{11} \quad \dots \quad \Psi_{44}] \tag{38}$$

$$[S] = \begin{bmatrix} N_1 & \dots & N_4 & 0 & \dots & 0 & \Phi_1 & \dots & \Phi_4 & 0 & \dots & 0 & \Psi_{11} & \dots & \Psi_{44} & 0 & \dots & 0 \\ 0 & \dots & 0 & N_1 & \dots & N_4 & 0 & \dots & 0 & \Phi_1 & \dots & \Phi_4 & 0 & \dots & 0 & \Psi_{11} & \dots & \Psi_{44} \end{bmatrix} \tag{39}$$

$$[S_1] = [N_{1,x} \quad \dots \quad N_{4,x} \quad N_{1,y} \quad \dots \quad N_{4,y} \quad \Phi_{1,x} \quad \dots \quad \Phi_{4,x} \quad \dots \quad \Phi_{4,y} \quad \Psi_{11,x} \quad \dots \quad \Psi_{44,x} \quad \Psi_{11,y} \quad \dots \quad \Psi_{44,y}] \tag{40}$$

$$[S_2] = \begin{bmatrix} N_{1,x} & \dots & N_{4,x} & 0 & \dots & 0 & \Phi_{1,x} & \dots & 0 & \dots & 0 & \Psi_{11,x} & \dots & \Psi_{44,x} & 0 & \dots & 0 \\ 0 & \dots & 0 & N_{1,y} & \dots & N_{4,y} & 0 & \dots & \Phi_{1,y} & \dots & \Phi_{4,y} & 0 & \dots & 0 & \Psi_{11,y} & \dots & \Psi_{44,y} \\ N_{1,y} & \dots & N_{4,y} & N_{1,x} & \dots & N_{4,x} & \Phi_{1,y} & \dots & \Phi_{1,x} & \dots & \Phi_{4,x} & \Psi_{11,y} & \dots & \Psi_{44,y} & \Psi_{11,x} & \dots & \Psi_{44,x} \end{bmatrix} \tag{41}$$



$$[S_3] = \begin{bmatrix} N_{1,x} & \dots & N_{4,x} & \Phi_{1,x} & \dots & \Phi_{4,x} & \Psi_{11,x} & \dots & \Psi_{44,x} \\ N_{1,y} & \dots & N_{4,y} & \Phi_{1,y} & \dots & \Phi_{4,y} & \Psi_{11,y} & \dots & \Psi_{44,y} \end{bmatrix} \quad (42)$$

$$\{Bf\} = \begin{Bmatrix} B_x \\ B_y \end{Bmatrix}, \quad \{Tf\} = \begin{Bmatrix} t_x^n \\ t_y^n \end{Bmatrix} \quad (43)$$

For plane strain state matrix  $[D]$  is defined by Eq. (44).

$$[D] = \frac{E}{(1+\nu)(1-2\nu)} \begin{bmatrix} 1-\nu & \nu & 0 \\ \nu & 1-\nu & 0 \\ 0 & 0 & (1-2\nu)/2 \end{bmatrix}. \quad (44)$$

### 2.2 Time integration

Maybe the most widely used family of direct methods for solving semi discrete equation of motion is the Newmark family which consists of the following equations [16]:

$$[M]\{\ddot{\Delta}_{n+1}\} + [C]\{\dot{\Delta}_{n+1}\} + [K]\{\Delta_{n+1}\} = \{Fr_{n+1}\} \quad (45)$$

$$\{\Delta_{n+1}\} = \{\Delta_n\} + \Delta t\{\dot{\Delta}_{n+1}\} + \Delta t^2(1/2 - \zeta)\{\ddot{\Delta}_n\} + \Delta t^2\zeta\{\ddot{\Delta}_{n+1}\} \quad (46)$$

$$\{\dot{\Delta}_{n+1}\} = \{\dot{\Delta}_n\} + \Delta t(1 - \gamma)\{\ddot{\Delta}_n\} + \Delta t\gamma\{\ddot{\Delta}_{n+1}\} \quad (47)$$

The Newmark family contains many well-known and widely used methods. The average acceleration method is one of them for structural dynamics applications which is unconditionally stable. In this method,  $\gamma$  and  $\zeta$  are equal to 1/2 and 1/4, respectively. We will choose the mean acceleration scheme, which is unconditionally stable, since for the partition of unity method with an explicit Newmark-type scheme, the stable time step of the enriched problem is a small fraction of the stable time step of the problem with no enriched shape function [11].

### 3 Interaction integral and SIF computations

In this section, the interaction integral is formulated by superimposing the actual and auxiliary fields on the path independent  $J$ -integral [30]. In this work, the non-equilibrium formulation [31] is used in conjunction with the XFEM to determine the  $M$ -integral for arbitrarily oriented cracks in FGMs under thermal and dynamic loading and also computation of the SIFs is explained in conjunction with the  $M$ -integral.

Now, we consider two independent admissible fields which are the actual  $(\mathbf{u}, \varepsilon, \sigma)$  and auxiliary  $(\mathbf{u}^{\text{aux}}, \varepsilon^{\text{aux}}, \sigma^{\text{aux}})$

fields. The  $J$ -integral of the superimposed fields (actual and auxiliary) can be written as follows:

$$J^s = \int_{A^*} \left\{ \left[ \left( \sigma_{ij} + \sigma_{ij}^{\text{aux}} \right) \left( u_{j,1} + u_{j,1}^{\text{aux}} \right) - 1/2 \left( \sigma_{jk} + \sigma_{jk}^{\text{aux}} \right) \left( \varepsilon_{jk}^m + \varepsilon_{jk}^{\text{aux}} \right) \delta_{1i} - 1/2 \rho \left( \dot{u}_k + \dot{u}_k^{\text{aux}} \right) \left( \dot{u}_k + \dot{u}_k^{\text{aux}} \right) \delta_{1i} \right] q_{,i} + \left[ \left( \sigma_{ij,i} + \sigma_{ij,i}^{\text{aux}} \right) \left( u_{j,1} + u_{j,1}^{\text{aux}} \right) + \left( \sigma_{ij} + \sigma_{ij}^{\text{aux}} \right) \left( u_{j,1i} + u_{j,1i}^{\text{aux}} \right) - 1/2 \left( \sigma_{ij} + \sigma_{ij}^{\text{aux}} \right) \left( \varepsilon_{ij,1}^m + \varepsilon_{ij,1}^{\text{aux}} \right) - 1/2 \left( \sigma_{ij,1} + \sigma_{ij,1}^{\text{aux}} \right) \left( \varepsilon_{ij}^m + \varepsilon_{ij}^{\text{aux}} \right) - \rho \left( \dot{u}_i + \dot{u}_i^{\text{aux}} \right) \left( \dot{u}_{i,1} + \dot{u}_{i,1}^{\text{aux}} \right) - 1/2 \rho_{,1} \left( \dot{u}_i + \dot{u}_i^{\text{aux}} \right) \left( \dot{u}_i + \dot{u}_i^{\text{aux}} \right) \right] q \right\} dA \quad (48)$$

where  $q$  is a weight function varying from unity at the crack tip to zero on boundary of domain  $A^*$  [31]. Equation (48) is decomposed into

$$J^s = J + J^{\text{aux}} + MI \quad (49)$$

where  $J$  and  $J^{\text{aux}}$  are given, respectively, by Eqs. (50) and (51).

$$J = \int_{A^*} \left\{ \left[ \sigma_{ij} u_{j,1} - 1/2 \sigma_{jk} \varepsilon_{jk}^m \delta_{1i} - 1/2 \rho \dot{u}_k \dot{u}_k \delta_{1i} \right] q_{,i} + \left[ \sigma_{ij,i} u_{j,1} + \sigma_{ij} u_{j,1i} - 1/2 \sigma_{ij} \varepsilon_{ij,1}^m - 1/2 \sigma_{ij,1} \varepsilon_{ij}^m - \rho \dot{u}_i \dot{u}_{i,1} - 1/2 \rho_{,1} \dot{u}_i \dot{u}_i \right] q \right\} dA \quad (50)$$

$$J^{\text{aux}} = \int_{A^*} \left\{ \left[ \sigma_{ij}^{\text{aux}} u_{j,1}^{\text{aux}} - 1/2 \sigma_{jk}^{\text{aux}} \varepsilon_{jk}^{\text{aux}} \delta_{1i} - 1/2 \rho \dot{u}_k^{\text{aux}} \dot{u}_k^{\text{aux}} \delta_{1i} \right] q_{,i} + \left[ \sigma_{ij,i}^{\text{aux}} u_{j,1}^{\text{aux}} + \sigma_{ij}^{\text{aux}} u_{j,1i}^{\text{aux}} - 1/2 \sigma_{ij}^{\text{aux}} \varepsilon_{ij,1}^{\text{aux}} - 1/2 \sigma_{ij,1}^{\text{aux}} \varepsilon_{ij}^{\text{aux}} - \rho \dot{u}_i^{\text{aux}} \dot{u}_{i,1}^{\text{aux}} - 1/2 \rho_{,1} \dot{u}_i^{\text{aux}} \dot{u}_i^{\text{aux}} \right] q \right\} dA \quad (51)$$

The resulting  $M$ -integral is given by

$$MI = \int_{A^*} \left\{ \left[ \sigma_{ij} u_{j,1}^{\text{aux}} + \sigma_{ij}^{\text{aux}} u_{j,1} - 1/2 \sigma_{jk}^{\text{aux}} \varepsilon_{jk}^{\text{aux}} \delta_{1i} - 1/2 \sigma_{jk}^{\text{aux}} \varepsilon_{jk}^m \delta_{1i} - \rho \dot{u}_k \dot{u}_k^{\text{aux}} \delta_{1i} \right] q_{,i} + \left[ \sigma_{ij,i} u_{j,1}^{\text{aux}} + \sigma_{ij,i}^{\text{aux}} u_{j,1} + \sigma_{ij} u_{j,1i}^{\text{aux}} + \sigma_{ij}^{\text{aux}} u_{j,1i} - 1/2 \sigma_{ij}^{\text{aux}} \varepsilon_{ij,1}^{\text{aux}} - 1/2 \sigma_{ij}^{\text{aux}} \varepsilon_{ij,1}^m - 1/2 \sigma_{ij,1}^{\text{aux}} \varepsilon_{ij}^{\text{aux}} - 1/2 \sigma_{ij,1}^{\text{aux}} \varepsilon_{ij}^m - \rho \dot{u}_i \dot{u}_{i,1}^{\text{aux}} - \rho \dot{u}_i^{\text{aux}} \dot{u}_{i,1} - \rho_{,1} \dot{u}_i \dot{u}_i^{\text{aux}} \right] q \right\} dA \quad (52)$$

Since the actual fields employ the quantities obtained from numerical simulation, the equilibrium and compatibility conditions are satisfied. For the auxiliary fields, the equilibrium condition is not satisfied [31], i.e.,  $\sigma_{ij,i}^{\text{aux}} \neq 0$ . While the relation between strain and displacement is compatible, i.e.,  $\varepsilon_{ij}^{\text{aux}} = 0.5(u_{i,j}^{\text{aux}} + u_{j,i}^{\text{aux}})$  and  $\sigma_{ij}u_{j,1i}^{\text{aux}} = \sigma_{ij}\varepsilon_{ij,1}^{\text{aux}}$ . The auxiliary stress field is defined as follows:

$$\sigma_{ij}^{\text{aux}} = C_{ijkl}(x)\varepsilon_{ij}^{\text{aux}} \tag{53}$$

Notice that the auxiliary fields are chosen as the asymptotic fields for homogeneous materials. Auxiliary fields, used in this paper, are based on Williams' solution [34] for stationary cracks and Swenson and Ingraffea [33] for moving cracks. Therefore, the resulting interaction integral (*MI*) becomes

$$\begin{aligned} MI = \int_{A^*} \left\{ \left[ \sigma_{ij}u_{j,1}^{\text{aux}} + \sigma_{ij}^{\text{aux}}u_{j,1} - \sigma_{jk}\varepsilon_{jk}^{\text{aux}}\delta_{1i} \right. \right. \\ \left. \left. - \rho\dot{u}_k\dot{u}_k^{\text{aux}}\delta_{1i} \right] q_{,i} + \left[ \rho\ddot{u}_j\dot{u}_{j,1}^{\text{aux}} + \sigma_{ij,i}^{\text{aux}}u_{j,1} \right. \right. \\ \left. \left. + \sigma_{ij}^{\text{aux}}(\alpha_{,1}\theta + \alpha\theta_{,1})\delta_{ij} - \left( C_{ijkl,1}\varepsilon_{kl}^m\varepsilon_{ij}^{\text{aux}} \right) \right. \right. \\ \left. \left. - \rho\dot{u}_i\dot{u}_{i,1}^{\text{aux}} - \rho\dot{u}_i^{\text{aux}}\dot{u}_{i,1} - \rho_{,1}\dot{u}_i\dot{u}_i^{\text{aux}} \right] q \right\} dA \tag{54} \end{aligned}$$

Since the numerical computation of displacements, strains, stresses, etc., is based on the global coordinate system, first the *M*-integral is evaluated in the global ( $MI_{\text{global}}$ ) and then transformed into the local coordinate system ( $MI_{\text{local}}$ ). The global *M*-integral quantities are evaluated by

$$\begin{aligned} (MI_n)_g = \int_{A^*} \left\{ \left[ \sigma_{ij}u_{j,n}^{\text{aux}} + \sigma_{ij}^{\text{aux}}u_{j,n} - \sigma_{jk}\varepsilon_{jk}^{\text{aux}}\delta_{ni} \right. \right. \\ \left. \left. - \rho\dot{u}_k\dot{u}_k^{\text{aux}}\delta_{ni} \right] \frac{\partial q}{\partial X_i} + \left[ \rho\ddot{u}_j\dot{u}_{j,n}^{\text{aux}} + \sigma_{ij,i}^{\text{aux}}u_{j,n} \right. \right. \\ \left. \left. + \sigma_{ij}^{\text{aux}}(\alpha_{,n}\theta + \alpha\theta_{,n})\delta_{ij} - \left( C_{ijkl,n}\varepsilon_{kl}^m\varepsilon_{ij}^{\text{aux}} \right) \right. \right. \\ \left. \left. - \rho\dot{u}_i\dot{u}_{i,n}^{\text{aux}} - \rho\dot{u}_i^{\text{aux}}\dot{u}_{i,n} - \rho_{,n}\dot{u}_i\dot{u}_i^{\text{aux}} \right] q \right\} dA, \quad n = 1, 2 \tag{55} \end{aligned}$$

where  $X_i$  denotes the global coordinate system (Fig. 2). The local *M*-integral quantity is given as [31].

$$MI_{\text{local}} = (MI_1)_{\text{global}} \cos \omega + (MI_2)_{\text{global}} \sin \omega \tag{56}$$

The relation between the *M*-integral and the SIFs for stationary crack in plane strain state is as follows:

$$MI_{\text{local}} = 2\left(1 - \nu_{\text{tip}}^2\right)\left(K_I K_I^{\text{aux}} + K_{II} K_{II}^{\text{aux}}\right) / E_{\text{tip}} \tag{57}$$

Also, for moving crack  $MI_{\text{local}}$  can be obtained from Eq. (58) [25].

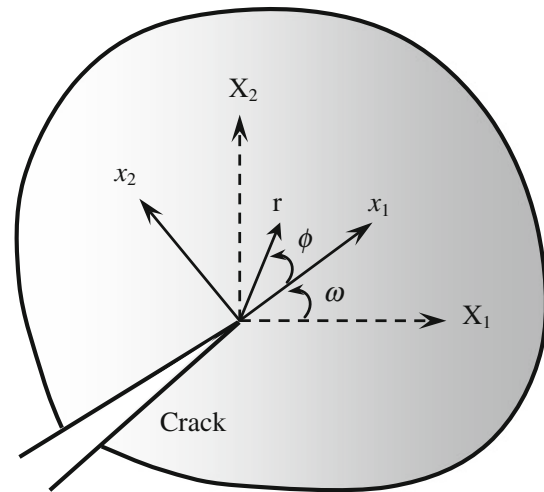


Fig. 2 Local (x1, x2) and global (X1, X2) coordinate systems

$$MI_{\text{local}} = 2\left(1 - \nu_{\text{tip}}^2\right)\left[\beta_1(\dot{a})K_I K_I^{\text{aux}} + \beta_2(\dot{a})K_{II} K_{II}^{\text{aux}}\right] / E_{\text{tip}} \tag{58}$$

where  $E_{\text{tip}}$  and  $\nu_{\text{tip}}$  denote Young's modulus and Poisson's ratio at crack tip, respectively, and  $\dot{a}$  is crack velocity.  $\beta_i$  are the universal functions (see Menouillard et al. [25]). Consequently,  $K_I$  and  $K_{II}$  are calculated by choosing  $K_I^{\text{aux}} = 1$ ,  $K_{II}^{\text{aux}} = 0$  and  $K_I^{\text{aux}} = 0$ ,  $K_{II}^{\text{aux}} = 1$ , respectively. The equivalent dynamic SIF  $K^{\text{eq}}$  is defined by Eq. (59) [25]:

$$K^{\text{eq}} = K_I \cos^3(\omega_c/2) - 1.5K_{II} \cos(\omega_c/2) \sin \omega_c \tag{59}$$

where  $\omega_c$  is the direction in which the crack will propagate from its current tip, and will be obtained using the maximum hoop stress criteria [25].

$$\begin{aligned} \omega_c = 2\arctan\left(0.25\left[K_I/K_{II} - \text{sign}(K_{II})\left((K_I/K_{II})^2 + 8\right)^{0.5}\right]\right), \\ -\pi < \omega_c < \pi \tag{60} \end{aligned}$$

In dynamic fracture mechanics, the initiation of growth and continued propagation of a crack depends on the equivalent SIF  $K^{\text{eq}}$  relative to the material critical SIF,  $K_{IC}$ . While  $K^{\text{eq}} < K_{IC}$ , the crack tip remains stationary. If  $K^{\text{eq}} \geq K_{IC}$ , the crack tip will be moved. In this paper, we use an algorithm similar to algorithm presented in Gerlach [11] to detect the crack propagation phenomenon.

#### 4 Modeling of functionally graded layer

The material properties of the functionally graded layer must be described across the layer thickness. In the present analysis, we assume that the material gradation is along the

$x$  direction and the volume fraction of inclusion follows a simple power function,

$$V_i(x) = (x/L)^p \tag{61}$$

where  $V_i$  is the volume fraction of inclusion and  $p$  is the power exponent determining the volume fraction profiles.

We assume that the functionally graded layer is made of metal-phase and ceramic-phase. In this study, we use micromechanical models for conventional composites given by Hatta and Taya [12] and Mori and Tanaka [27] to calculate the properties of functionally graded ceramics (FGCs). Also, the fracture toughness of the two-phase FGC composite needs to be determined. Here, we adopt Jin and Batra's [17] rule of mixtures formula for a two-phase FGC composite.

$$K_{IC}(x) = \left\{ V_1(x)(K_{IC}^1)^2 + V_2(x)(K_{IC}^2)^2 \right\}^{1/2} \tag{62}$$

To incorporate these relations into the XFE model, first the value of each material property is calculated at each individual node based on micromechanical models. Then, material properties at each Gaussian integration point can be interpolated from the nodal material properties of the element using isoparametric shape functions which are the same for spatial coordinates ( $x, y$ ). Thus, material properties such as elastic modulus ( $E$ ), Poisson's ratio ( $\nu$ ), and mass density ( $\rho$ ) at Gauss points can be interpolated using shape functions from nodal points as [20]

$$E = \sum_{i=1}^h N_i E_i, \quad \nu = \sum_{i=1}^h N_i \nu_i, \quad \rho = \sum_{i=1}^h N_i \rho_i, \tag{63}$$

$h = 1, 2, \dots, ne.$

### 5 Numerical examples

In this section, first we present two numerical examples which examine the accuracy and precision of presented method in this paper. Then we consider the effect of volume fraction profile of FGMs and initial crack angle on crack tip SIFs in next example. In the last example, we study the crack propagation phenomenon in a FG layer under thermal shock. The plane strain state is assumed in all numerical examples.

#### 5.1 First example

We consider an elastic two-dimensional isotropic and homogeneous layer with an edge crack (Fig. 3). The initial temperature  $T_0$  is chosen to be 400 K. The layer is rapidly cooled by conduction at its left surface to  $T_1$ , which is

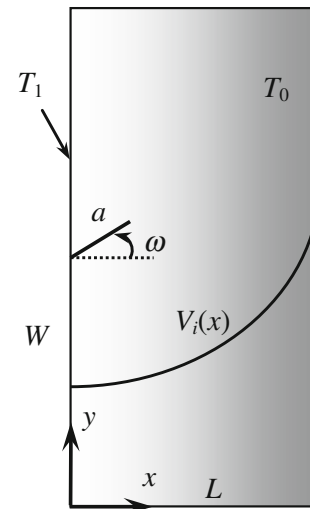


Fig. 3 Geometry and boundary condition of the layer

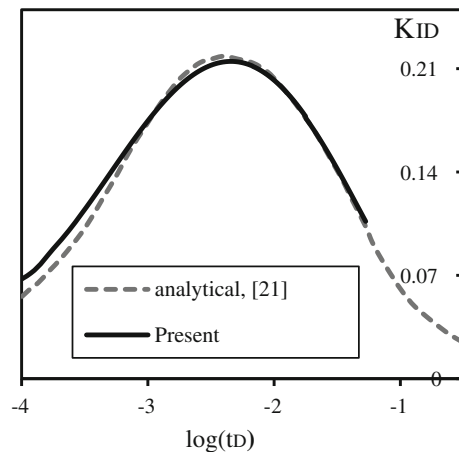


Fig. 4 Normalized SIF versus logarithm of normalized time for first numerical example

equal to 350 K in this study. All other sides are assumed to be thermally insulated.

The problem dimensions are  $L = 0.001$  m,  $W = 0.002$  m,  $a = 0.00005$  m and  $\omega = 0$  (Fig. 3). The material properties are  $\rho = 5,600$  kg/m<sup>3</sup>,  $E = 117$  GPa,  $\nu = 0.333$ ,  $\alpha = 7.118 \times 10^{-6}$  K<sup>-1</sup>,  $c_t = 615.6$  J/(kg K) and  $k = 2.036$  W/m K. A  $51 \times 101$  four-node rectangular element mesh is used and the selected time step is  $\Delta t = 10^{-4}$  s. The analytical [21] and numerical dimensionless SIF ( $K_{ID}$ ) is plotted versus the logarithm of dimensionless time ( $t_D$ ) in Fig. 4, where good accordance is observed. In this example, we define  $K_{ID}$  and  $t_D$  which follow from Eqs. (64) and (65).

$$K_{ID} = K_I(1 - \nu) / \{ E\alpha(T_0 - T_1)L^{0.5} \} \tag{64}$$

$$t_D = kt / \rho c_t L^2. \tag{65}$$

5.2 Second example

A FG two-dimensional layer with a horizontal edge crack is considered, as shown in Fig. 3. The layer is initially at a constant temperature. Without loss of generality, the initial temperature can be assumed to be 200 K. The layer is suddenly cooled down by conduction at its left surface to temperature  $T_1$ , which is equal to 190 K. The initial and boundary conditions for the temperature field are:

$$\begin{aligned} T &= 200 \text{ K at } t = 0 \\ T &= 190 \text{ K at } x = 0 \\ T &= 200 \text{ K at } x = L \end{aligned} \tag{66}$$

We suppose that the heat transfer coefficient on the surfaces of the FGM strip is infinite which is an idealized thermal shock boundary condition. The problem dimensions are  $L = 0.001$  m and  $W = 0.002$  m (Fig. 3). Two crack lengths are considered in this example,  $a = 0.0001$  m and  $a = 0.0003$  m. The mesh consists of  $61 \times 121$  four-node rectangular element in this example and the selected time step is  $\Delta t = 2 \times 10^{-4}$  s.

Table 1 lists the properties of the constituent materials, i.e.,  $\text{Al}_2\text{O}_3$  and  $\text{Si}_3\text{N}_4$ . This study assumes that the volume fraction of  $\text{Si}_3\text{N}_4$  (phase  $i$ ) follows a simple power function (Eq. (61)). The material gradation in the  $x$  direction is considered.

The SIFs for this two-dimensional thermoelasticity problem are compared with those obtained by Jin and Paulino [18] in Fig. 5 which shows a good agreement between both results.

Figure 5 illustrates that under thermal shock, increasing the crack length will decrease the SIF. The dimensionless

thermal SIF at the crack tip and dimensionless time can be computed as follows:

$$K_{\text{ID}} = K_{\text{I}}(1 - \nu) / \left\{ E\alpha_0(T_0 - T_1)(\pi L)^{0.5} \right\} \tag{67}$$

$$t_{\text{D}} = k_0 t / \rho_0 c_{10} L^2. \tag{68}$$

5.3 Third example

In this example, first we consider the effects of volume fraction profile of FGMs and the initial crack angle on the crack tip SIFs.

Dimensions and boundary conditions of considered layer are identical to the first example. The initial temperature  $T_0$  is chosen to be 500 K and a thermal shock equal to  $-50^\circ$  ( $\theta = -50$ ) is applied to left surface of layer. The initial length of crack is  $a = 0.0001$  m. Identical to previous example, in these numerical calculations, we consider an alumina/silicon nitride ( $\text{Al}_2\text{O}_3/\text{Si}_3\text{N}_4$ ) FGM which is used in cutting tool applications (see Table 1). The thermally shocked surface is pure  $\text{Al}_2\text{O}_3$  as in cutting tool applications. The material gradation in the  $x$  direction is considered and the volume fraction of  $\text{Si}_3\text{N}_4$  follows than Eq. (61). A mesh with  $61 \times 121$  four-node rectangular element is used and the selected time step is  $\Delta t = 10^{-4}$  s.

To study the effect of the material gradation, the coupled thermoelasticity problem with three different values of  $p$  is analyzed (i.e.,  $p = 0.5$ ,  $p = 1$  and  $p = 2$ ). The time variations of the normalized mode-I thermal dynamic SIF (for the chosen gradient parameter  $p$ ) are shown in Fig. 6. Equations (67) and (68) are used for normalization of the time and the SIFs. Figure 6 illustrates that increasing the material gradient parameter ( $p$ ) will increase the SIFs.

**Table 1** Material properties of  $\text{Al}_2\text{O}_3$  and  $\text{Si}_3\text{N}_4$  [7]

	Young's modulus (GPa)	Poisson's ratio	CTE ( $10^{-6} \text{ K}^{-1}$ )	Thermal conductivity (W/m K)	Mass density ( $\text{kg/m}^3$ )	Specific heat (J/kg K)	Fracture toughness ( $\text{MPa m}^{1/2}$ )
$\text{Al}_2\text{O}_3$	320	0.25	8	20	3,800	900	4
$\text{Si}_3\text{N}_4$	320	0.25	3	35	3,200	700	5

**Fig. 5** Normalized SIF versus normalized time for second numerical example, **a**  $a/L = 0.1$ , **b**  $a/L = 0.3$

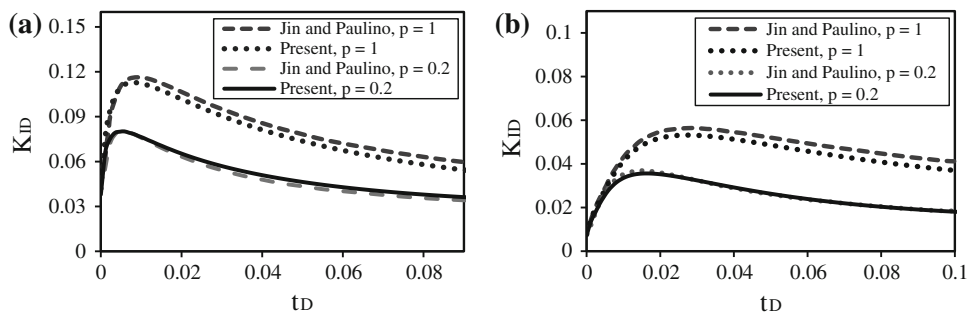


**Fig. 6** Normalized SIFs versus normalized time for third example, **a** horizontal crack, **b** and **c** oblique crack

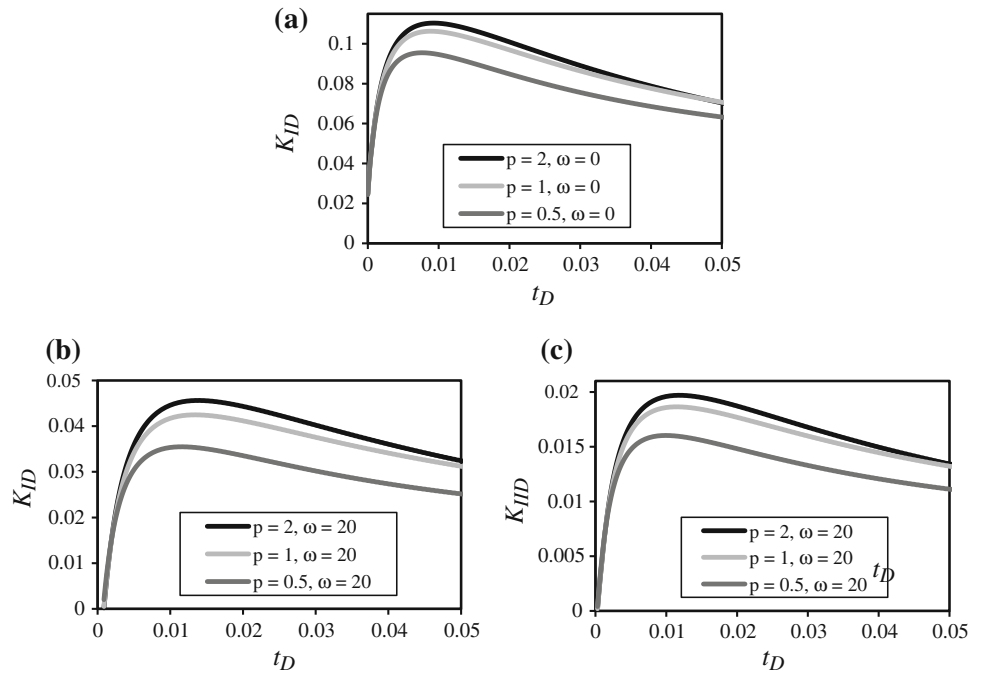
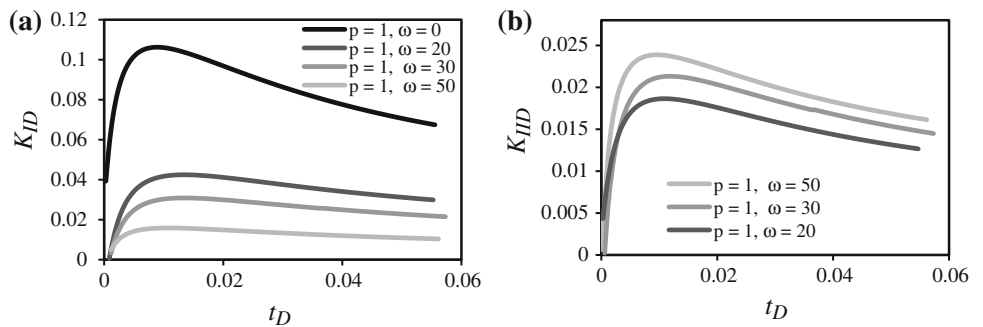


**Fig. 7** Normalized SIFs versus normalized time for third example, **a**  $K_I$ , **b**  $K_{II}$



The influence of the initial crack angle on the values of  $K_I$  and  $K_{II}$  are shown in Fig. 7a and b, respectively. These figures demonstrate that regardless of the material gradation, increasing the crack angle will decrease  $K_I$  and will increase  $K_{II}$ .

#### 5.4 Fourth example

In this example, we study the crack propagation phenomenon in a FG layer with a horizontal edge crack under thermal shock. Dimensions, properties, mesh and boundary conditions of considered layer are identical to the previous example. The initial temperature  $T_0$  is chosen to be 800 K. A thermal shock equal to  $-500^\circ$  ( $\theta = -500$ ) is applied to left surface of layer which is higher than its critical value for considered layer. The initial crack length is equal to 0.0001 m. Figure 8 illustrates von Mises stress contours for a layer with  $p = 1$  at threshold of crack growth (Fig. 8a) and after  $t = 0.0024$  s (Fig. 8b). Deformed shapes of this

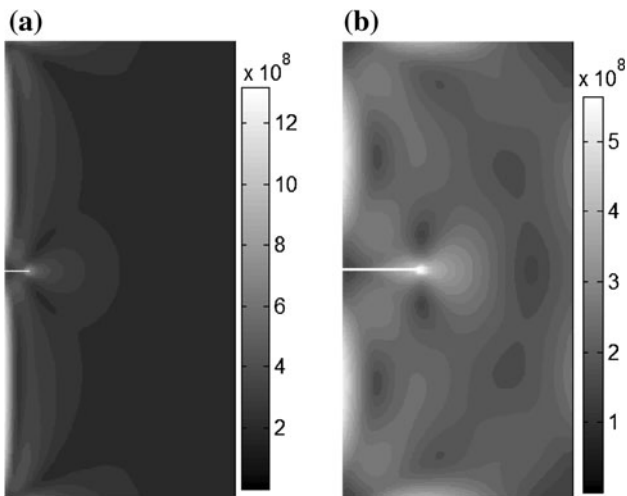


**Fig. 8** Von Mises stress contours for a layer with  $p = 1$  at: **a** threshold of crack growth, **b** after  $t = 0.0024$  s

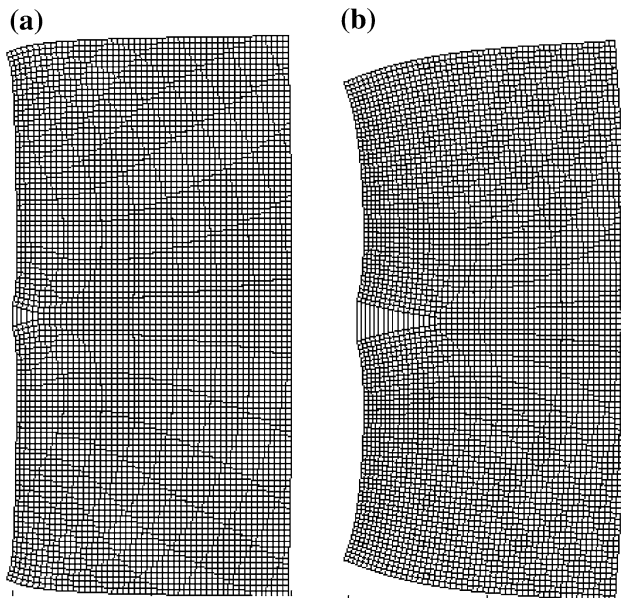


**Fig. 9** Deformed shape of cracked FG layer, **a** threshold of crack growth, **b** after 0.0024 s

layer at mentioned times, are presented in Fig. 9. For more clarification, displacements are multiplied by 50 in plotting this figure.

We find from numerical simulations that the mean crack propagation velocities for FG layers with  $p = 0.5, 1$  and  $2$  are about  $0.115, 0.14$  and  $0.16$  m/s, respectively. In fact, increasing the material gradient parameter ( $p$ ) will increase the crack propagation velocity. Also, obtained results show that the crack arrest occurs earlier in the layer with smaller  $p$ .

## 6 Conclusions

In this study, classical coupled thermoelastic equations were solved using the XFE and the Newmark methods in FGMs. The most general form of interaction integral were developed to evaluate dynamical SIFs for both homogenous and FG materials. Also, the crack propagation phenomenon is considered in a FG layer under thermal shock. Finally, the following results were obtained from this study:

1. If a thermal shock is imposed to the cracked face of a FG layer, increasing the crack length will decrease the SIF.
2. Under thermal shock, increasing the material gradient parameter ( $p$ ) in a FG Layer will increase the SIFs.
3. For a FG layer under thermal shock, regardless of the material gradation, increasing the crack angle will decrease  $K_I$  and will increase  $K_{II}$ .
4. Under thermal shock, increasing the material gradient parameter ( $p$ ) in a FG Layer will increase the crack propagation velocity.

5. Increasing material gradient parameter ( $p$ ) will increase crack propagation velocity. Also, the crack arrest occurs earlier in layer with smaller  $p$ .

## References

1. Azadi M, Azadi M (2009) Nonlinear transient heat transfer and thermoelastic analysis of thick walled FGM cylinder with temperature dependent material properties using Hermitian transfinite element. *J Mech Sci Technol* 23:2635–2644
2. Bao G, Cai H (1997) Delamination cracking in functionally graded coating/metal substrate systems. *Acta Mater* 45(3): 1055–1066
3. Belytschko T, Moës N, Usui S, Parimi C (2001) Arbitrary discontinuities in finite elements. *Int J Numer Methods Eng* 50(4):993–1013
4. Black T, Belytschko T (1999) Elastic crack growth in finite elements with minimal remeshing. *Int J Numer Methods Eng* 45:601–620
5. Duflo M (2008) The extended finite element method in thermoelastic fracture mechanics. *Int J Numer Methods Eng* 74:827–847
6. Ekhlov AV, Khay OM, Zhang Ch, Sladek J, Sladek V (2012) A BDEM for transient thermoelastic crack problems in functionally graded materials under thermal shock. *Comput Mater Sci* 57:30–37
7. Feng Y, Jin Z (2009) Thermal fracture of functionally graded plate with parallel surface cracks. *Acta Mech Solida Sin* 22(5):453–464
8. Fujimoto T, Noda N (2000) Crack propagation in a functionally graded plate under thermal shock. *Arch Appl Mech* 70(6): 377–386
9. Fujimoto T, Noda N (2001) Two crack growths in a functionally graded plate under thermal shock. *J Therm Stress* 24:847–862
10. Gaudette FG, Giannakopoulos AE, Suresh S (2001) Interface cracks in layered materials subjected to a uniform temperature change. *Int J Fract* 110(4):325–349
11. Gerlach CA (1999) “omputational methods for the dynamic response of cracked specimens. PhD thesis, Northwestern university, Evanston, IL
12. Hatta H, Taya M (1986) Equivalent inclusion method for steady state heat conduction in composites. *Int J Eng Sci* 24:520–524
13. Hetnarski RB, Eslami MR (2009) Thermal stresses—advanced theory and applications. Springer, Berlin
14. Hosseini-Tehrani P, Eslami MR, Daghyani HR (2001) Dynamic crack analysis under coupled thermoelastic assumption. *J Appl Mech* 68(4):584–588
15. Hosseini-Tehrani P, Hosseini-Godarzi AR, Tavangar M (2005) Boundary element analysis of stress intensity factor KI in some two dimensional dynamic thermoelastic problems. *Eng Anal Bound Elem* 29:232–240
16. Hughes TJR (1987) The finite element method. Prentice-Hall, Englewood Cliffs
17. Jin Z-H, Batra RC (1996) Some basic fracture mechanics concepts in functionally graded materials. *J Mech Phys Solid* 44:1221–1235
18. Jin Z-H, Paulino GH (2001) Transient thermal stress analysis of an edge crack in a functionally graded material. *Int J Fract* 107:73–98
19. KC A, Kim J-H (2008) Interaction integrals for thermal fracture of functionally graded materials. *Eng Fract Mech* 75:2542–2565

20. Kim J-H, Paulino GH (2002) Isoparametric graded finite elements for nonhomogeneous isotropic and orthotropic materials. *ASME J Appl Mech* 69:502–514
21. Lee KY, Sim KB (1990) Thermal shock stress intensity factor by Bueckner's weight function method. *Eng Fract Mech* 37(4): 799–804
22. Lee YD, Erdogan F (1998) Interface cracking of FGM coatings under steady-state heat flow. *Eng Fract Mech* 59(3):361–380
23. Lee YD, Erdogan F (1995) Residual/thermal stresses in FGM and laminated thermal barrier coatings. *Int J Fract* 69:145–165
24. Melenk JM, Babuška I (1996) The partition of unity finite element method: basic theory and applications. *Comput Methods Appl Mech Eng* 139(1–4):289–314
25. Menouillard T, Song J-H, Duan Q, Belytschko T (2010) Time dependent crack tip enrichment for dynamic crack propagation. *Int J Fract* 162:33–49
26. Moës N, Dolbow J, Belytschko T (1999) A finite element method for crack growth without remeshing. *Int J Numer Methods Eng* 46(1):131–150
27. Mori T, Tanaka K (1973) Average stress in matrix and average elastic energy of materials with misfitting inclusions. *Acta Mater* 21:571–574
28. Noda N (1997) Thermal stress intensity factor for functionally gradient plate with an edge crack. *J Therm Stress* 20(3–4): 373–387
29. Quian G, Nakamura T, Berndt CC (1998) Effects of thermal gradient and residual stresses on thermal barrier coating fracture. *Mech Mater* 27:91–110
30. Rice JR (1968) A path-independent integral and the approximate analysis of strain concentration by notches and cracks. *ASME J Appl Mech* 35(2):379–386
31. Song SH, Paulino GH (2006) Dynamic stress intensity factors for homogeneous and smoothly heterogeneous materials using the interaction integral method. *Int J Solid Struct* 43:4830–4866
32. Stolarska M, Chopp DL, Moës N, Belytschko T (2001) Modeling crack growth by level sets in the extended finite element method. *Int J Numer Methods Eng* 51:943–960
33. Swenson DV, Ingraffea AR (1988) Modeling mixed-mode dynamic crack propagation using finite elements: theory and applications. *Comput Mech* 3:381–397
34. Williams ML (1957) On the stress distribution at the base of a stationary crack. *ASME J Appl Mech* 24(1):109–114
35. Zamani A, Eslami MR (2009) Coupled dynamical thermoelasticity of a functionally graded cracked layer. *J Therm Stress* 32:969–985
36. Zamani A, Eslami MR (2010) Implementation of the extended finite element method for dynamic thermoelastic fracture initiation. *Int J Solid Struct* 47:1392–1404